

Simple Maps in Accelerator Simulations

Ubaldo Iriso*, Stephen Peggs†
Brookhaven National Laboratory, Upton, NY

Abstract

Maps are powerful tools in the study of dynamical systems that are intrinsically discrete in time. Difference systems described by maps exhibit much richer dynamical behavior than differential systems, because of the emphasis they intrinsically place on occasional “high-frequency” transient kicks. For example, the standard map – with pulsed gravity – displays chaos, while the analogous gravity pendulum does not. Maps also speed up simulations enormously, by summarizing complex dynamics in short form. Accelerator physics offers a variety of such systems, like RF systems (represented by the standard map) and motion in the presence of sextupoles (Henon map). This paper summarizes the state of the art of cubic maps used to simulate electron clouds, and coupled maps used to simulate interacting electron and ion clouds. Coupled maps are capable of demonstrating the first order phase transitions (from cloud “off” to “on” or vice versa) that are sometimes seen in practice, and enable the practical extension of electron cloud simulations to include relatively slowly evolving ion clouds.

INTRODUCTION

Logistic map

The simplest and most famous map is probably the logistic map, given by

$$Y_{m+1} = \alpha Y_m (1 - Y_m) \quad (1)$$

where, in one interpretation, Y_m is the population of a particular species. Propagation from one year m to the next $m + 1$ depends on the success of a single breeding season, with exponential growth for small Y if the control parameter α is greater than 1. It also depends on starvation through the competition for resources among a large population, represented by the negative quadratic term in Y^2 . The population quickly converges on an equilibrium value of

$$Y^* = \frac{\alpha - 1}{\alpha} \quad (2)$$

if $1 < \alpha < 2$, but first oscillates around that value if $2 < \alpha < 3$. Period-2 oscillations are observed for $3 < \alpha < 1 + \sqrt{6}$, with further bi-furcation at larger values. The onset of chaos occurs at values of $\alpha \geq 3.57$ – slight variations in the initial population lead to very different population evolutions.

* email: ubaldo.iriso@cells.es

† email: peggs@bnl.gov

Henon map

Poincare discovered the topic of chaos in the late 19th century, in the context of celestial mechanics [1]. Nonetheless, it was only with the advent of relatively powerful computers that interest and knowledge in the field exploded. One of the earliest of the recent investigators was Henon, an astrophysicist [2]. The map that now bears his name can be written as

$$\begin{pmatrix} x \\ x' \end{pmatrix}_{m+1} = R(2\pi Q_x) \left[\begin{pmatrix} x \\ x' \end{pmatrix}_m + \begin{pmatrix} 0 \\ x^2 \end{pmatrix}_m \right] \quad (3)$$

where, in an accelerator interpretation, x and x' are normalized horizontal phase space co-ordinates, R is the rotation matrix and Q_x is the horizontal betatron tune. The nonlinear quadratic term on the right represents a single thin sextupole that is encountered just before linear motion from turn m to turn $m + 1$. Despite its deceptively simple form, this map displays all the features of fully detailed accelerator tracking codes, such as detuning, regular resonant trajectories, rapidly divergent regular trajectories and, of course, chaos [3, 4].

Standard map

The motion of a pendulum is (approximately) simulated by using the standard map

$$\begin{aligned} \theta_{m+1} &= \theta_m + \Delta t \theta'_m \\ \theta'_{m+1} &= \theta'_m - \Delta t \sin(\theta_{m+1}) \end{aligned} \quad (4)$$

where θ and θ' represent the angle and the angular velocity of the pendulum. Here Δt is the time that elapses from integration step m to $m + 1$. Eq. 4 can be written in differential form as

$$\frac{d^2\theta}{dt^2} = -\delta(t - n \Delta t) \Delta t \sin(\theta) \quad (5)$$

where the delta function causes gravity to be “pulsed on” for all integer values of n . Numerical artifacts – such as chaos and resonance locking – are introduced into the simulated motion of a pendulum, unless $\Delta t \ll 1$.

On the contrary, these “artifacts” are real if Eq. 4 (accurately) represents longitudinal motion in an accelerator where a single thin RF cavity is encountered once per turn. In this case θ_m is the RF phase and θ'_m is (proportional to) the off-momentum parameter $\Delta p/p$. The synchrotron tune for small amplitude oscillations Q_s is then related to Δt through

$$\cos(2\pi Q_s) = 1 - \frac{\Delta t^2}{2} \quad (6)$$

Chaos abounds in much of longitudinal phase space when $Q_s \geq 0.15$. It is the “violence” of an occasional delta function transient that introduces additional rich dynamics.

Cubic maps for electron clouds

Quasi-stationary seed electrons in the vacuum pipe of an accelerator are violently accelerated to an energy of order 1 keV each time that a short bunch of positive particles passes by. These electrons strike the vacuum pipe wall, rapidly dissipating and diffusing into an electron spectrum that has a typical energy of only a few eV, until the next bunch passes by, when the process is iterated. Figure 1 illustrates the average energy at which the electrons strike the chamber wall between two bunch passages, from a CSEC [5] simulation for two different bunch intensities in RHIC: $N = 4 \times 10^{10}$ (red circles) and $N = 12 \times 10^{10}$ protons (blue squares). Electrons receive a boost during the bunch passage (black trace), but the average energy decreases approximately exponentially until the next bunch arrives.

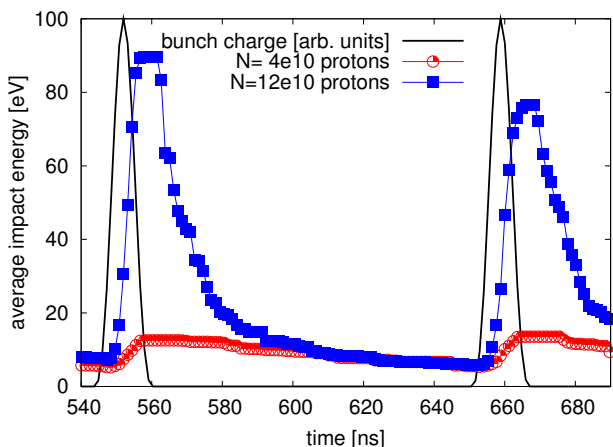


Figure 1: Average energy at which the electrons strike the wall between two bunch passages. Electrons receive a boost from the bunch passage, but they rapidly dissipate into slow motion [6].

The average electron cloud charge density ρ initially grows exponentially as a train of bunches passes by, until space charge effects “starve” further growth, and saturated equilibrium is attained. A typical evolution is shown in Figure 2, from a CSEC simulation with 60 bunches of 1.4×10^{11} protons circulating in the RHIC ring, with a bunch spacing of 107 ns. The red line shows CSEC output, while the black circles mark the average electron density between the passage of two bunches, whether full or empty. The main features of electron cloud build-up – or decay – are well represented by the “bunch-by-bunch” evolution. Thus, it is sufficient to take a single sample (average) of the electron cloud once per bunch passage, even though the details of the evolution between two bunches are lost. The

natural unit of time is one bunch passage.

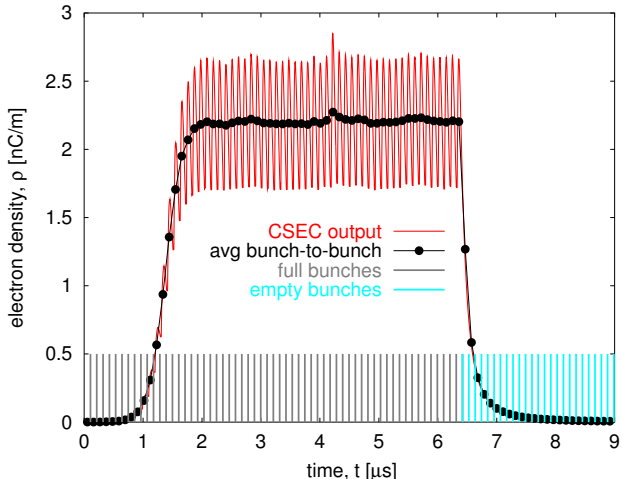


Figure 2: Time evolution of the electron density (red line) computed with CSEC during $9 \mu\text{s}$ (RHIC time revolution is $12.82 \mu\text{s}$). The case corresponds to the injection of 60 successive bunches with a bunch spacing of 107 ns and a bunch intensity of $N = 1.4 \times 10^{11}$ protons (marked with black bars), followed by 60 “empty” bunches (marked with light blue bars). The black circles mark the average electron density between two consecutive bunches [7].

The bunch-by-bunch evolution of the electron cloud from m to $m + 1$ is accurately represented by a cubic map

$$\rho_{m+1} = a\rho_m + b\rho_m^2 + c\rho_m^3, \quad (7)$$

where ρ [nC/m] is the linear electron cloud density [7, 6]. Other mapping expressions are also possible, but the cubic map seems optimal [7]. Exponential growth of weak electron clouds occurs if $a > 1$.

Coupled maps for interacting clouds

It is conjectured below that the interplay between electron clouds and (partially ionized) ion clouds is important. This interplay is expressed by the general map

$$\begin{aligned} \rho_{m+1} &= f(\rho_m, R_m) \\ R_{m+1} &= g(\rho_m, R_m), \end{aligned} \quad (8)$$

where R_m [nC/m] is the ion cloud density after the passage of the m 'th bunch. (Both ρ and R are defined to be positive, here.) For example, the following “proof-of-principle” coupled maps are considered [8, 6]:

$$\begin{aligned} \rho_{m+1} &= (a + yR_m)\rho_m + b\rho_m^2 + c\rho_m^3 \\ R_{m+1} &= AR_m + Y\rho_m \end{aligned} \quad (9)$$

If the coupling coefficients are turned off ($y = Y = 0$), then the cubic electron cloud map Eq. 7 is recovered, along with the uncoupled ion map

$$R_{m+1} = AR_m. \quad (11)$$

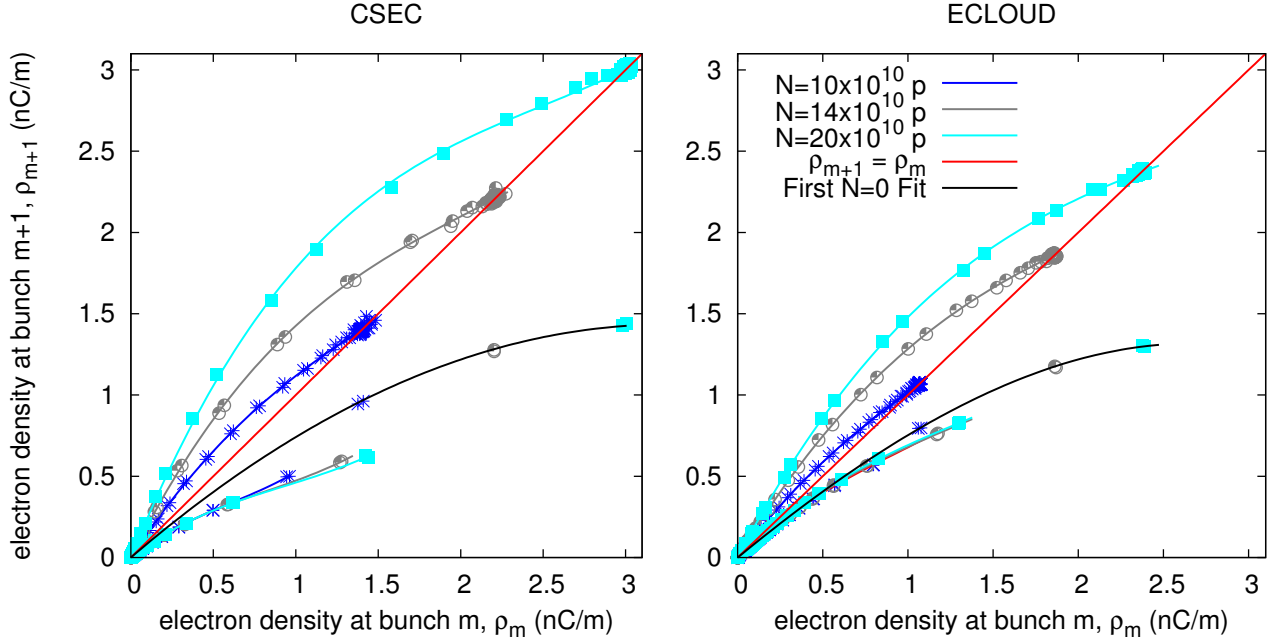


Figure 3: Average electron density after bunch passage m , ρ_{m+1} , as a function of the electron density before bunch m passed by, ρ_m , for different bunch intensities, N . The left plot shows the CSEC output, while the points on the right hand side come from ECLLOUD simulation. In both cases, the lines correspond to cubic fits applied to the average bunch to bunch points [7].

The slow clearing of ion clouds through the action of vacuum pumping occurs (in the absence of other mechanisms) for values of A slightly less than unity.

ELECTRON CLOUD PHENOMENOLOGY

The fast simulation code MEC

Figure 3 shows cubic fits to electron cloud build up in the space (ρ_m, ρ_{m+1}) for different bunch intensities, N , using data from two different simulation codes, CSEC and ECLLOUD. The fast simulation code MEC (*Maps for Electron Cloud*) uses these cubic maps to simulate the bunch-by-bunch evolution of the electron cloud density. The use of MEC is divided into four cases, depending on the intensity of bunches m and $m-1$:

- “Off-On”: A full bunch follows an empty one, i.e. $N_m = N_0$ and $N_{m-1} = 0$, with cubic map coefficients represented by the vector: $\vec{A}_{10} = (a_{10}, b_{10}, c_{10})$.
- “On-On”: Two full bunches, with $N_m = N_0$ protons and $N_{m-1} = N_0$. The cubic map coefficients for this case are denoted by $\vec{A}_{11} = (a_{11}, b_{11}, c_{11})$.
- “Off-Off”: An empty bunch follows a full bunch, i.e. $N_m = 0$ and $N_{m-1} = N_0$. The corresponding cubic map coefficients are represented by $\vec{A}_{01} = (a_{01}, b_{01}, c_{01})$.

- “Off-Off”: Two empty bunches, with bunches of intensity $N_m = 0$ and $N_{m-1} = 0$. The corresponding cubic map coefficients are denoted by $\vec{A}_{00} = (a_{00}, b_{00}, c_{00})$.

Figure 4 shows that MEC successfully reproduces the bunch-to-bunch evolution simulated by CSEC for a variety of bunch patterns. The largest difference for the maximum density is about 15%, while for the average density the maximum difference is about 17%. However, CSEC uses about 1 h CPU time for each case, while MEC uses only ~ 1 ms – a speed up of seven orders of magnitude!

The optimum bunch train distribution

Maps codes like MEC are much faster than brute force simulations like CSEC and ECLLOUD (between 6 and 7 orders of magnitude). Maps also offer a level of abstraction that can lead to conclusions otherwise difficult to obtain. For example: given a fixed number of bunches with a given beam intensity, what is the optimum bunch distribution along the bunch train to minimize the electron cloud density? Maps not only enable fast simulations to assist in answering this question: they also enable a semi-analytical approach using a linear approximation that is valid at small cloud densities [7, 6].

MEC requires four sets of polynomial coefficients, $\vec{A}_{11}(N)$, $\vec{A}_{01}(N)$, $\vec{A}_{00}(N)$ and $\vec{A}_{10}(N)$, to follow the bunch to bunch evolution of the electron cloud density.

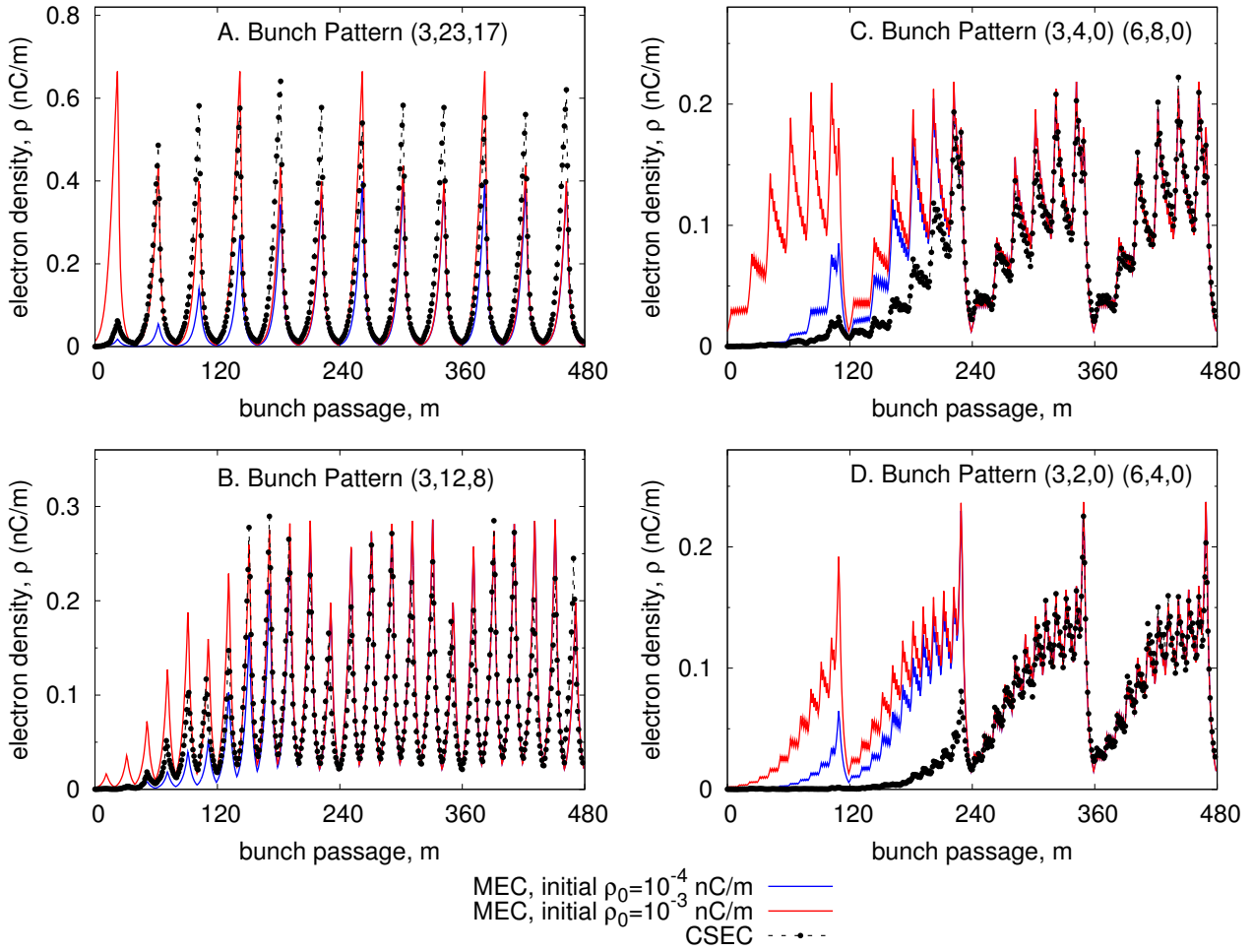


Figure 4: Electron cloud density evolution for four different bunch patterns using CSEC (dashed black trace with dots) and MEC with two different initial electron densities: $\rho_0 = 10^{-4}$ nC/m (blue line) and $\rho_0 = 10^{-3}$ nC/m (red line). No matter the initial electron density, MEC results agree for the last turn (from bunch passage 360 to 480) within an error range of about 15% for all bunch patterns. See Ref. [7].

Considering small electron densities, one can approximate the evolution of the electron density to be linear in the (ρ_m, ρ_{m+1}) space. That is, if there is a total number of M bunches in a ring with a “bunch harmonic” number of H , the linearization of the problem gives a one turn map that is simply:

$$\rho_{m+H} \approx F(N) \rho_m \quad (12)$$

where the F is the “one turn factor” [7],

$$F = \left(\frac{a_{10} a_{01}}{a_{11} a_{00}} \right)^i \left(\frac{a_{11}}{a_{00}} \right)^M a_{00}^H \quad (13)$$

and i is the number of transitions from full to empty (and empty to full) bunches. In general the minimum possible number of transitions is $i = 1$ (if all the bunches are clumped together), and the maximum number of transitions is the smaller of M and $H - M$ (when the bunches are

spread as sparsely as possible). The special case $i = 0$ applies when there is no abort gap, $M = H$.

If $F > 1$ then the electron cloud density increases to some saturated value, while if $F < 1$ then the cloud disappears. For given M , H and N , the smallest (largest) value of F occurs for the largest (smallest) allowed value of i if

$$\left(\frac{a_{10} a_{01}}{a_{11} a_{00}} \right) < 1 \quad (14)$$

and vice versa. Since Eq. 14 is valid for RHIC parameters, the most sparse distribution of a fixed number of fixed population bunches is the most stable against electron cloud growth.

Analytical derivation of the linear map coefficient a

The dependence of the map parameters (a, b, c) on the physical parameters of interest (bunch intensity, bunch

length, secondary emission yield, bunch spacing, beam pipe size, etc) can be empirically derived from brute force simulations codes like CSEC or ELOUD. It is also possible to derive (at least) the linear map coefficient a semi-analytically.

A key ingredient determining electron cloud build up is δ , the secondary emission yield (SEY), which has two components:

- δ_r : secondary electrons produced after an elastic collision of the primary electron with the chamber wall. Their energy is the same as the energy of the primary electrons.
- δ_t : “true” secondary electrons, which come from electrons that penetrated few tens of nanometers into the chamber material and are emitted at low energy, $E_{\text{sec}} \sim 5$ eV.

Based on these considerations, an expression for the linear map coefficient a is found from first principles [6, 9]:

$$a = \int_0^\infty \left[\delta_r(E)^{n(E)} + \delta_t(E) \delta_{\text{sec}}^{\xi(E)} \frac{\delta_{\text{sec}}^{n(E)\xi(E)} - \delta_r^{n(E)}}{\delta_{\text{sec}}^{\xi(E)} - \delta_r(E)} \right] h(E) dE \quad (15)$$

where $h(E)$ is the energy distribution of the electrons after their acceleration due to the bunch passage, $\xi(E) = \sqrt{E/E_{\text{sec}}}$, $\delta_{\text{sec}} = \delta(E_{\text{sec}})$ and $n(E)$ denotes the number of collisions that an electron at energy E has between two bunch passages. From this expression, it is compelling to call the parameter a the **effective secondary emission yield** of the beam pipe wall, δ_{eff} , depending on both the chamber material and the beam characteristics. Electron clouds are triggered if a (or δ_{eff}) is greater than one.

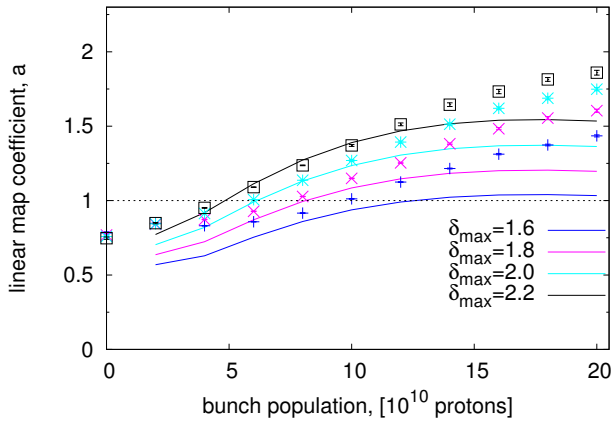


Figure 5: Comparison of the linear map coefficient a derived using CSEC simulations (symbols) and using Eq. 15 (lines), as a function of the bunch population N for different values of δ_{max} [6].

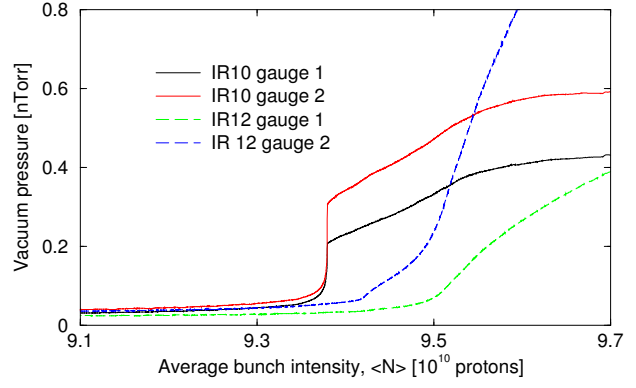


Figure 6: First and second order electron cloud phase transitions observed in the interaction regions IR10 and 12 of the RHIC. The data were taken as the bunch population slowly decayed during beam fill 5905. The actual copper ion bunch population is converted to an equivalent average number of protons per bunch [8, 6].

Figure 5 compares the results of calculations of the linear map coefficient a using this analytical method (lines) and after fitting the CSEC simulation results (symbols) as a function of the bunch population and for different δ_{max} (maximum value of δ). The color of the symbols and lines coincide for the same δ_{max} . Both results agree acceptably in the general evolution of the parameter a . The largest disagreement occurs when $N > 12 \times 10^{10}$ protons per bunch, perhaps because of the neglect of the re-diffused electrons, which might play an important role when the energy gain E_g due to the bunch passage is larger than the energy at which the SEY has its maximum, E_{max} .

First order phase transitions

After electron cloud formation, what happens as the bunch population slowly decays? Do the electron clouds collapse suddenly, or do they slowly fade away? After an electron cloud formation, equilibrium is obtained when $\rho_{m+1} = \rho_m \equiv \rho^*$. For example, if the cubic term in c is negligible, then the equilibrium electron density is

$$\rho^* = \begin{cases} 0 & ; \text{ when } a < 1 \\ \frac{a-1}{-b} & ; \text{ when } a > 1. \end{cases} \quad (16)$$

For a fixed set of beam pipe parameters, the coefficient a increases monotonically with the bunch population N (see Figure 5). From Eq. 16, it then follows that the phase transition from electron cloud “off” to “on” is second order – $\rho^*(N)$ increases smoothly from zero above a critical threshold population, when $a > 1$. Complex simulation codes consistently reproduce only second order phase transitions [10].

However, experimental data shown in Figure 6 illustrate how both first and second order phase transitions are seen in RHIC, as a threshold bunch population is crossed. While

the pressure in IR12 smoothly decreases as the bunch population slowly drops, an abrupt transition is seen in IR10. Pressure and electron density are proportionally related [11, 12], and a first order phase transition in pressure indicates a first order phase transition in the electron density, as shown in Ref. [8]. This catastrophic collapse of the pressure is unexpected, especially since the surface parameters show a smooth dependence on the impact electron energy at the wall [13, 14]. The failure of simulations to reproduce these first order phase transitions, and of theory to predict them, indicates that there is missing physics in the modeling.

Interactions between negative electron clouds and partially ionized positive ion clouds [15, 16, 17] are a candidate for such additional physics [8]. Simulations of the interplay between electron clouds and ion clouds face two main challenges. First, there are a significant number of uncertain surface physics parameters for both electron and ions. Second, ion cloud dynamics are extremely slow compared to electron cloud dynamics, resulting in prohibitively long CPU times for contemporary brute force simulation codes.

Maps can be used to circumvent the second of these challenges, thereby providing an improved intuitive understanding of the coupled evolution of electron and ion clouds [8, 6]. Coupled maps also show how, at least in principle, first order phase transitions can occur.

INTERACTING ELECTRON AND ION CLOUDS

In the following, we use the vector \vec{r} for the electron and ion densities

$$\vec{r}_m = \begin{pmatrix} \rho_m \\ R_m \end{pmatrix}. \quad (17)$$

A fixed point is found when

$$\vec{r}_{m+1} = \vec{r}_m \equiv \vec{r}^*. \quad (18)$$

Linearized motion close to the fixed point is given by

$$\vec{r}_{m+1} = J(\vec{r}_m - \vec{r}^*) + \vec{r}^* \quad (19)$$

where J is the 2x2 Jacobian matrix

$$J = \begin{pmatrix} \frac{\partial f}{\partial \rho_m} & \frac{\partial f}{\partial R_m} \\ \frac{\partial g}{\partial \rho_m} & \frac{\partial g}{\partial R_m} \end{pmatrix}_{\vec{r}^*}, \quad (20)$$

for the general coupled map introduced in Eq. 8.

For the fixed point to be stable, small perturbations must result in an evolution that converges back towards it. This occurs if one of the two following pairs of conditions is fulfilled:

$$i) \quad t^2 < d^2 \quad ; \quad \text{and} \quad d^2 < 1 \quad (21)$$

$$ii) \quad t^2 > d^2 \quad ; \quad \text{and} \quad |t| + \sqrt{t^2 - d^2} < 1, \quad (22)$$

where the convenient definitions $t \equiv \text{Tr}(J^2)/2$, and $d \equiv \det(J)$ have been introduced [8]. If neither of these conditions applies, then the motion diverges, and the fixed point is unstable.

A numerical example

Assume that all the coupled map coefficients are constants except for the bunch to bunch electron cloud gain, a . From the fitting results in Ref. [7, 6], we presume that a depends linearly on the bunch population according to

$$a = 0.4 + 0.1 (N/10^{10}). \quad (23)$$

The coupled map coefficient values used throughout below and quoted in Table 1 are illustrative – they are not intended to quantitatively reproduce RHIC results.

Table 1: Map parameters used in the following examples.

a	b	c	y	A	Y
Eq. 23	-0.1	-0.08	0.4	0.96	0.03

Three fixed electron densities exist for $N = 5.0 \times 10^{10}$ protons/bunch: $\rho_1^* = 0$ nC/m, $\rho_2^* = 0.69$ nC/m and $\rho_3^* = 1.81$ nC/m. Calculating the Jacobian matrix at the three solutions, their corresponding stability is obtained using Eqs. 21 and 22. This is illustrated in Figure 7, which depicts the motion around these solutions. Consistently with the stability conditions in Eqs. 21 and 22 and expressed in-situ in the corresponding plot, the first solution $\vec{r}^*_{*1} = (0, 0)$ shows an elliptical converging motion, the second solution $\vec{r}^*_{*2} = (0.69, 0.52)$ exhibits a hyperbolic divergence, and the third solution $\vec{r}^*_{*3} = (1.81, 1.357)$ shows a hyperbolic converging motion.

The presence of a coupled ion cloud enhances the electron survival, and stable and non-zero electron clouds are created even when $a < 1$. Enhanced electron survival due to the presence of an ion cloud is also considered in Ref. [18], but the ion cloud density is not allowed to evolve. The importance of the model stems from its ability to show the possibility of abrupt transitions even with a smooth dependence of the map coefficients on electron cloud parameters (such as bunch population or length). Recall that all coefficients remain constant except $a(N)$, which changes linearly with the bunch intensity.

First order phase transitions and hysteresis

These conditions lead to a first order phase transition, and to hysteresis [8, 6]. Figure 8 shows the results of a dynamical simulation in which the coupled maps are applied directly, first as the bunch population is slowly decreased, and then as it is slowly increased. The solid line shows that the stable electron cloud density decreases as the bunch population is reduced, until at $N \approx 4.7 \times 10^{10}$ the electron cloud collapses catastrophically. When the bunch population is then slowly increased, no electron (or ion) cloud forms up to a population of $N = 6.0 \times 10^{10}$, when the cloud grows rapidly to a stable stationary value.

Figure 9 shows the flow in (ρ, R) space for different bunch populations: $N = 3, 5$ and 7×10^{10} protons/bunch. These plots result from tracking several simulations with different initial conditions. For $N = 3 \times 10^{10}$ (left plot),

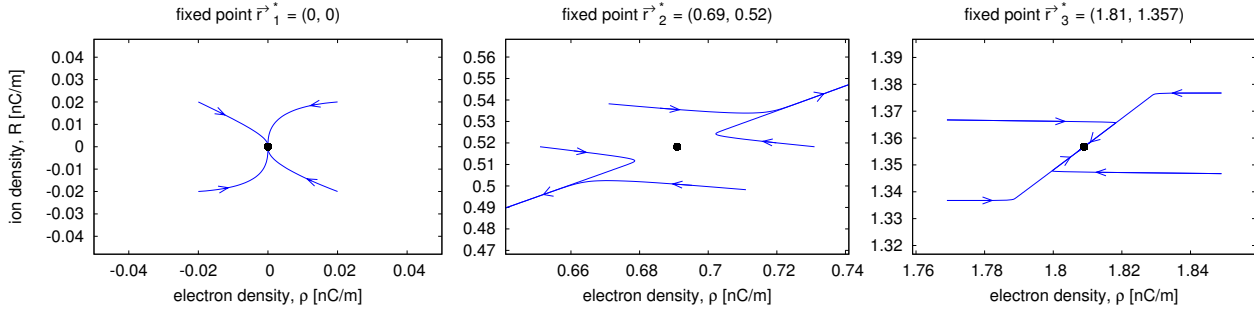


Figure 7: Stability around the 3 fixed points for $N = 5 \times 10^{10}$ protons/bunch. The second solution (middle plot) shows a hyperbolic diverging motion, through which small perturbations around the fixed point $r_{*2}^{\vec{r}}$ diverge quickly towards $r_{*1}^{\vec{r}}$ or $r_{*3}^{\vec{r}}$, depending on the initial conditions. The first (left) and the third solution (right plot) show a converging motion that attracts all the points in its vicinity. Recall that only trajectories with positive ρ, R are physically sensible; the motion depicted around $r_{*1}^{\vec{r}}$ includes negative values of ρ and R only as a numerical example [8, 6].

all trajectories are attracted to the *global attractor* at the $r_{*}^{\vec{r}} = (0, 0)$ fixed point. Similar behavior is found for $N = 7 \times 10^{10}$ (right plot), where all trajectories converge to the *global attractor* at $r_{*}^{\vec{r}} = (2.9, 2.17)$, no matter what initial conditions are used. Note that there is also a fixed point *global repeller* at $r_{*}^{\vec{r}} = (0, 0)$.

However, the situation is different for $N = 5 \times 10^{10}$ protons/bunch (middle plot in Figure 9). Two different *basins of attraction* coexist: one corresponding to the fixed point $r_{*}^{\vec{r}} = (0, 0)$, the second corresponding to the fixed point $r_{*}^{\vec{r}} = (1.81, 1.357)$. This feature (different attractors depending on the initial conditions) is the origin of the hysteresis and the first order phase transitions.

In this model the presence of either first or second order phase transitions depends on the values of the map coefficients, which produce ion cloud densities compara-

ble to electron cloud densities, $\rho \sim R$. The importance of the model stems from its ability to show the possibility of abrupt transitions even with a smooth dependence of the map coefficients on electron cloud parameters (such as bunch population or length). Recall that in this numerical example all coefficients remain constant except a , which changes linearly with the bunch intensity.

Figure 10 shows the evolution of the electron and ion clouds for different bunch populations, always starting with the same (arbitrary) initial cloud densities. The clouds decay away or build to stable solutions with $N = 3 \times 10^{10}$ or 6×10^{10} protons per bunch respectively, consistent with classical expectations (see Figure 8). However, the clouds evolve into a stable period-2 oscillation when $N = 9 \times 10^{10}$ protons/bunch. Chaos is encountered with $N = 12 \times 10^{10}$ protons/bunch.

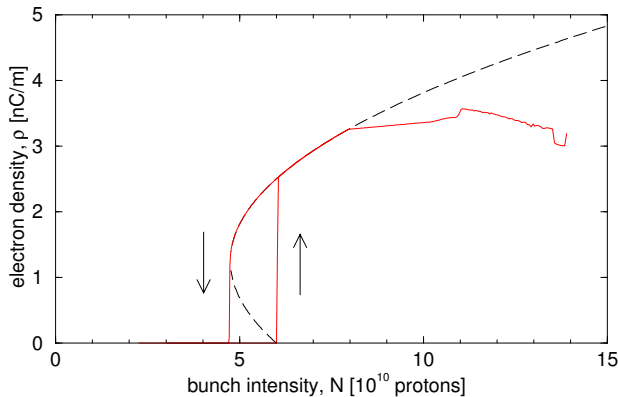


Figure 8: Evolution of the electron cloud density as the bunch population N is first slowly decreased, and then slowly increased. The precipitous and hysteretic behavior is characteristic of first order phase transitions. The dashed lines represent the two stationary solutions described by the uncoupled electron cloud map [8, 6].

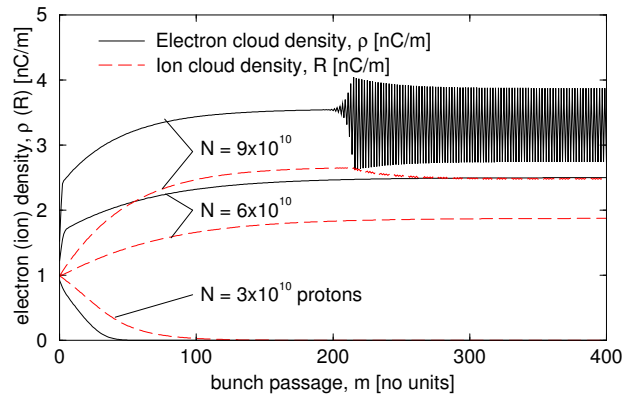


Figure 10: Dynamical evolution of the electron and ion cloud densities as a function of time (bunch passage number) for 3 different bunch intensities, $N = 3 \times 10^{10}$, 6×10^{10} , and 9×10^{10} protons/bunch.

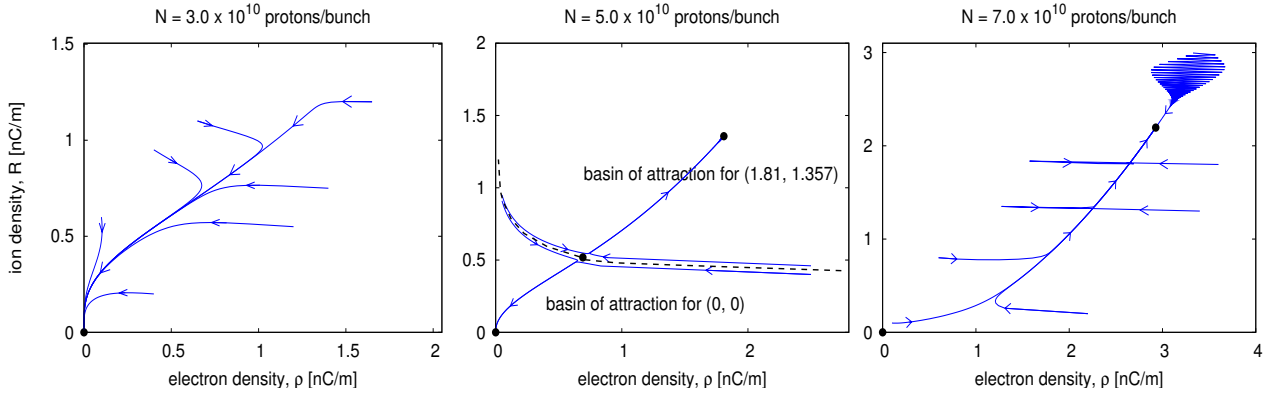


Figure 9: Coupled motion in (ρ, R) space is tracked following the coupled maps for $N = 3 \times 10^{10}$ protons/bunch (left plot), $N = 5 \times 10^{10}$ protons/bunch (middle plot), and $N = 7 \times 10^{10}$ protons/bunch (right plot). Only one fixed point – $\vec{r}^* = (0, 0)$ – exists for $N = 3 \times 10^{10}$, which acts as a global attractor. There are two *basins of attraction* for $N = 5 \times 10^{10}$: one containing the fixed point $\vec{r}^*_{1} = (0, 0)$, and the second containing $\vec{r}^*_{3} = (1.81, 1.357)$. The fixed point $\vec{r}^*_{2} = (0.69, 0.52)$ sits on the boundary between the two basins, acting as a global repeller, and the system evolve towards \vec{r}^*_{1} or \vec{r}^*_{3} , depending on the initial conditions. The fixed point $\vec{r}^* = (2.9, 2.17)$ is a global attractor for $N = 7 \times 10^{10}$ protons/bunch, all trajectories converge to this point as $m \rightarrow \infty$, and the fixed point $(0, 0)$ is a repeller [8, 6].

CONCLUSIONS

Simple maps (difference equations) are inherently richer than analogous differential equations in the dynamical behavior that they display. Maps enhance the generation of period doubling and chaos, because of the transient violence of a nonlinear restoring force that is pulsed on once per unit of time. In the case of accelerators – where “thin” elements like sextupoles, RF cavities or electron clouds are encountered once per turn – this behavior is real, rather than artifact.

Simulations representing complex physics can sometimes be summarized in short form by a map representation. For example, electron cloud growth and decay in RHIC and in the LHC is accurately described by a simple cubic map. The quantities of interest then become the control parameters – the map coefficients – and their dependence on physical parameters (in this case bunch population, bunch length, bunch spacing, secondary emission yield and bunch spacing, et cetera). Semi-analytical derivation of the control parameters is possible, for example the linear electron cloud coefficient a , which can also be called the effective secondary emission yield.

In addition to enabling a more abstract focus on control parameters, a map approach to electron clouds also has the practical advantage of enabling simulation speed up by 6 or 7 orders of magnitude. This speed up is even more important when turning to investigate interactions between electron clouds and partially ionized ion clouds, because brute force simulations of ion cloud dynamics require even more time CPU time.

Conventional electron cloud simulations reproduce only second order phase transitions from cloud-off to cloud-on. Interactions between electron and ion clouds are conjec-

tured as one way that additional physics can be introduced, in order to reproduce the first order phase transitions sometimes seen in practice. Coupled maps representing this interaction can not only reproduce first order phase transitions (and hysteresis), but suggest that additional dynamical behavior – such as period doubling and even chaos – are possible in practice. Such additional dynamical phases have not (yet) been observed in electron clouds in accelerators, but it is possible they occur at, or near, typical operating conditions. An understanding of coupled cloud dynamics from the map perspective may prove important in enhancing accelerator performance.

ACKNOWLEDGMENTS

We wish to acknowledge the support of many people in the Collider-Accelerator Department at Brookhaven National Laboratory, including M. Blaskiewicz, W. Fischer, R. Hseuh, and S.Y. Zhang. We would like to especially thank the effort of P. Thieberger for his support and his enlightening discussions.

REFERENCES

- [1] *Les Methods Nouvelle de la Mechanique Celeste*, H. Poincare, Gautier Vilars, Paris, 1892.
- [2] M. Henon, Q. Appl. Math 2:291, 1969.
- [3] *Nonlinear Problems in Accelerator Physics*, S. Peggs and R. Talman, Ann. Rev. Nucl. Part. Sci, 36:287-325, 1986.
- [4] *Iteration and Accelerator Dynamics*, S. Peggs, SSC-144, Dallas, 1987.
- [5] *How to run CSEC*, M. Blaskiewicz and U. Iriso, BNL Internal Report C-AD/AP/XXX, Upton, October 2006.

- [6] *Electron Clouds in the Relativistic Heavy Ion Collider*, U. Iriso, PhD Thesis, University of Barcelona, January 2006.
- [7] *Maps for electron clouds* U. Iriso and S. Peggs, PRST-AB 8, 024403 (2005).
- [8] *Maps for coupled electron and ion clouds in accelerators* U. Iriso and S. Peggs, Phys. Rev. ST Accel. Beams 9, 071002 (2006).
- [9] *Analytic calculation of the electron cloud linear map coefficient* U. Iriso and S. Peggs, Proceedings of EPAC'06, June 2006.
- [10] *Electron cloud phase transitions*, U. Iriso and S. Peggs, C-AD/AP/147, Upton, April 2004.
- [11] *Electron induced molecular desorption from electron clouds at the Relativistic Heavy Ion Collider*, U. Iriso and W. Fischer, Phys. Rev. ST Accel. Beams 8, 113201 (2005).
- [12] *Properties of the electron cloud in a high-energy positron and electron storage ring*, K. Harkay and R.A. Rosenberg, Phys. Rev. ST Accel. Beams 6, 034402 (2003).
- [13] M.A. Furman and M. Pivi, Microscopic probabilistic model for the simulation of secondary electron emission, PRST-AB 5, 124404, (2002).
- [14] R. Cimino, I. Collins, M. Furman, M. Pivi, F. Ruggiero, G. Rumolo, F. Zimmermann, Can low energy electrons affect high energy accelerators? Phys. Rev. Lett. **93**, 014801 (2004).
- [15] G. Rumolo and F. Zimmermann, Interplay of Ionization and Sputtering with the electron cloud, CERN-SL-2001-014 AP, 2001.
- [16] *Electron Cloud driven vacuum instability*, W. Fischer, U. Iriso, and E. Mustafin. Proc. of ICFA Workshop on High Intensity and High Brightness Hadron Beams, Bensheim, October 2004.
- [17] *Vacuum aspects for an LHC upgrade*, O. Gröbner, Proc. of CARE HHH-2004 Workshop, Geneva, November 2004.
- [18] *Maps, electron-clouds in RHIC and first-order phase-transitions*. P. Thieberger, U. Iriso, and S. Peggs, C-A/AP/197.